Geophysical Journal International

Advancing Astronomy and Grophysics

doi: 10.1093/gji/ggy074

Geophys. J. Int. (2018) 213, 1969–1983 Advance Access publication 2018 February 23 GJI Geomagnetism, rock magnetism and palaeomagnetism

A field like today's? The strength of the geomagnetic field 1.1 billion years ago

Courtney J. Sprain,* Nicholas L. Swanson-Hysell, Luke M. Fairchild and Kevin Gaastra[†]

Department of Earth and Planetary Science, University of California, Berkeley, CA 94720, USA. E-mail: C.Sprain@liverpool.ac.uk

Accepted 2018 February 21. Received 2018 February 13; in original form 2017 June 2

SUMMARY

Palaeomagnetic data from ancient rocks are one of the few types of observational data that can be brought to bear on the long-term evolution of Earth's core. A recent compilation of palaeointensity estimates from throughout Earth history has been interpreted to indicate that Earth's magnetic field strength increased in the Mesoproterozoic (between 1.5 and 1.0 billion years ago), with this increase taken to mark the onset of inner core nucleation. However, much of the data within the Precambrian palaeointensity database are from Thellier-style experiments with non-ideal behaviour that manifests in results such as double-slope Arai plots. Choices made when interpreting these data may significantly change conclusions about long-term trends in the intensity of Earth's geomagnetic field. In this study, we present new palaeointensity results from volcanics of the ~1.1-billion-year-old North American Midcontinent Rift. While most of the results exhibit non-ideal double-slope or sagging behaviour in Arai plots, some flows have more ideal single-slope behaviour leading to palaeointensity estimates that may be some of the best constraints on the strength of Earth's field for this time. Taken together, new and previously published palaeointensity data from the Midcontinent Rift yield a median field strength estimate of 56.0 ZAm²—very similar to the median for the past 300 Myr. These field strength estimates are distinctly higher than those for the preceding billion years (Ga) after excluding ca. 1.3 Ga data that may be biased by non-ideal behaviour—consistent with an increase in field strength in the late Mesoproterozoic. However, given that \sim 90 per cent of palaeointensity estimates from 1.1 to 0.5 Ga come from the Midcontinent Rift, it is difficult to evaluate whether these high values relative to those estimated for the preceding billion years are the result of a stepwise, sustained increase in dipole moment. Regardless, palaeointensity estimates from the Midcontinent Rift indicate that the surface expression of Earth's geomagnetic field at ~ 1.1 Ga may have been similar to that on the present-day Earth.

Key words: Core; North America; Dynamo: theories and simulations; Magnetic field variations through time; Palaeointensity; Palaeomagnetism.

1 INTRODUCTION

Earth's solid inner core grows by the freezing of liquid iron from the outer core (Jacobs 1953). This process provides power to the geodynamo through the release of light elements and latent heat during crystallization, which contributes to convection in the liquid outer core, and results in a sustained magnetic field (Verhoogen 1961). Estimates for the timing of initial growth of Earth's inner core are

strongly dependent upon the thermal conductivity of the core (Olson 2013; Labrosse 2015). Recent experiments and calculations (de Koker *et al.* 2012; Pozzo *et al.* 2012) suggest that the thermal conductivity of the core is significantly larger than previously assumed, in which case the transfer of heat at the core—mantle boundary must be higher than previously thought. An implication of this higher heat flux is that inner core formation is likely to be younger, with updated estimates from modified thermal evolution models often being less than 1 billion years (Ga; Gomi *et al.* 2013; Davies 2015; Labrosse 2015; Ohta *et al.* 2016), compared to previous estimates which were as old as ~3.5 Ga (Gubbins *et al.* 2004). Such a young age for inner core formation may require that there were additional power sources to the geodynamo through the Proterozoic (e.g. Badro *et al.* 2016; O'Rourke & Stevenson 2016; Hirose *et al.* 2017; O'Rourke *et al.* 2017). However, these new thermal conductivity values for

^{*}Now at: Geomagnetism Laboratory, Department of Earth, Ocean and Ecological Sciences, School of Environmental Sciences, University of Liverpool, Liverpool, L69 7ZE, UK.

[†]Now at: Department Earth, Environmental and Planetary Science, Rice University, Houston, TX 77005, USA.

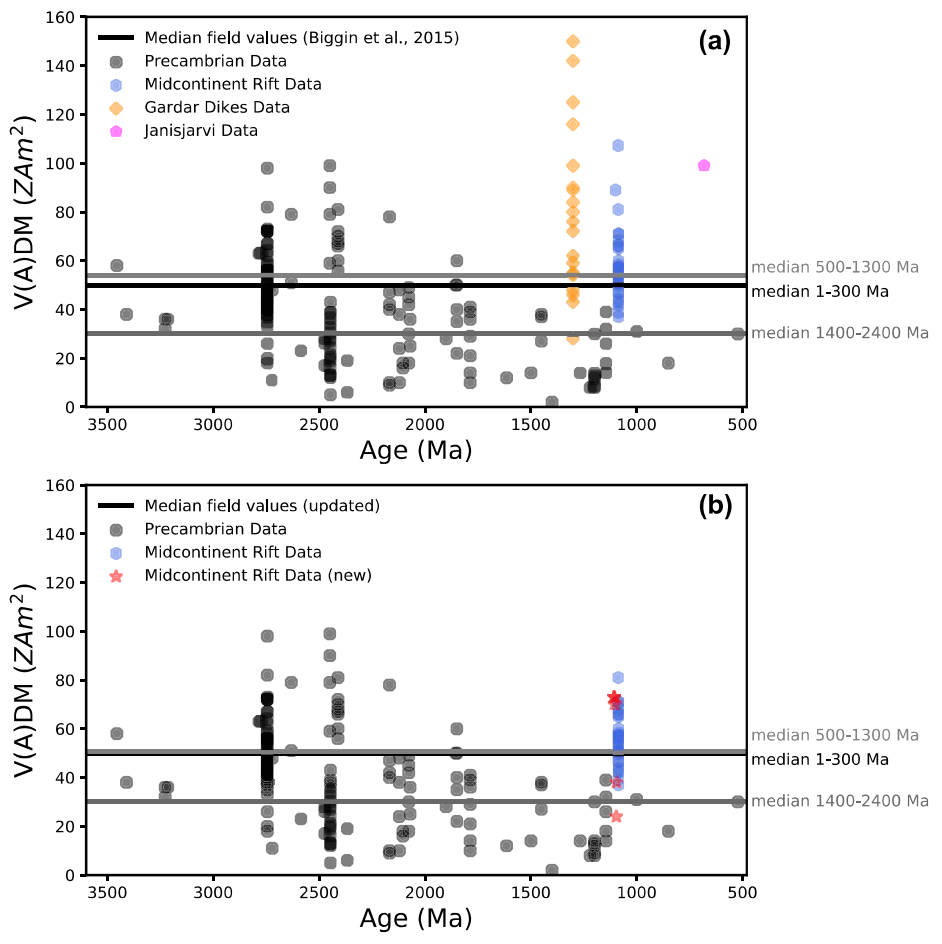


Figure 1. (a) Site-mean V(A)DMs with $Q_{\text{Pl}} \geq 3$ used in Biggin *et al.* (2015) for the Precambrian. Blue hexagons mark data from the Midcontinent Rift, orange diamonds mark data from the Gardar volcanics and a pink pentagon marks data from the Jänisjärvi impact. Grey and black lines indicate median values for Early, Middle and Late bins as reported in Biggin *et al.* (2015). (b) Same as (a), but excluding low-temperature/high-slope data from the Midcontinent Rift, Gardar volcanics and Jänisjärvi impact, and including new estimates from this study (red stars). Grey and black lines indicate median values for early, middle and late bins calculated from this study.

the core are not universally accepted and estimates continue to vary (Konôpková *et al.* 2016; Ohta *et al.* 2016). Obtaining an independent estimate of the timing of inner core formation would constrain the thermal evolution of the core and mantle, in addition to improving our understanding of the history of Earth's dynamo.

Given that the nucleation of the inner core would have introduced a new power source to the dynamo, a hypothesized indicator of this change at Earth's surface is an increase in the intensity of the geomagnetic field (Stevenson et al. 1983; Aubert et al. 2009; Biggin et al. 2009). Driscoll (2016) proposed a scenario based on a suite of numerical dynamo simulations where there are four core dynamo regimes associated with this thermal evolution: (i) a multipolar strong-field dynamo before \sim 1.7 Ga, (ii) a strong-field, dominantly axial dipolar dynamo between 1.7 and 1.0 Ga, (iii) a weak-field dynamo, where the dipole field is generally not axially aligned, between 1.0 and 0.6 Ga and then (iv) a strong-field, axial dipolar field from ~0.6 Ga to present with the return to a strong-field dynamo initiated by nucleation of the inner core. The numerical dynamo simulations of Landeau et al. (2017) show that such a weak-field regime is possible prior to nucleation of the inner core, but exists within a narrow parameter space such that a sustained dipole-dominated dynamo was likely present before and after the nucleation of the inner core. The numerical results of Landeau et al. (2017) also show little change in surface dipole moment associated

with the nucleation of the inner core. While the formation of the inner core adds an additional power source for the geodynamo, it also results in the dynamo region being deeper in the core in these simulations. A shallower dynamo with magnetic energy density closer to the core—mantle boundary prior to inner core nucleation results in a similar surface dipole moment to that generated once the core was solidifying in the Landeau *et al.* (2017) simulations. Therefore, an increase in surface dipole moment is a possible, but not definite, outcome of inner core nucleation.

A recent compilation of palaeointensity data filtered using the $Q_{\rm Pl}$ quality criteria of Biggin & Paterson (2014) was interpreted to indicate that Earth's magnetic field strength increased in the Mesoproterozoic (between 1.5 and 1.0 Ga; Fig. 1a), with this increase suggested to mark the onset of inner core nucleation (Biggin *et al.* 2015). As in previous compilations of palaeointensity estimates from Precambrian rocks (Biggin *et al.* 2009; Valet *et al.* 2014), Biggin *et al.* (2015) interpreted the intensity of Earth's magnetic field to have been low for much of the Palaeoproterozoic into the Mesoproterozoic, with this period of low dipole moment sandwiched between periods of higher magnetic field intensity. Hypothesized core dynamics behind these regimes are: vigorous thermal convection resulting from high core—mantle heat flux during early Earth history followed by a period of weaker thermal convection as the heat flux fell, and then a transition to a geodynamo primarily

driven by compositional convection and a return to higher field values once inner core nucleation initiated (Biggin et al. 2009). The timing of inner core nucleation interpreted by Biggin et al. (2015) is older than that implied by thermal evolution models utilizing high core thermal conductivity values (e.g. Labrosse 2015), which could suggest intermediate values of thermal conductivity with significant implications for Earth's thermal evolution. However, the Mesoproterozoic increase in field strength that is interpreted to mark the onset of inner core nucleation in the Biggin et al. (2015) compilation is based on limited data, dominantly from two localities: (1) the \sim 1.1. Ga North American Midcontinent Rift, and (2) the \sim 1.3 Ga Gardar lava flows from Greenland. Taken together, data from these two igneous provinces constitute 75 per cent of the sites within the $Q_{PI} \ge 3$ 'Late' (1300–500 Ma) bin of Biggin *et al.* (2015). It has been argued by Smirnov et al. (2016) that some data from these localities overestimate the true field strength due to non-ideal behaviour during Thellier-style palaeointensity experiments.

A standard method for palaeointensity determination is the Thellier double-heating technique. Thellier-type palaeointensity experiments consist of stepwise heating, in the presence (in-field) and absence (zero-field) of an applied magnetic field, in order to progressively replace the natural remanent magnetization (NRM) with a partial thermal remanent magnetization (pTRM, Thellier & Thellier 1959). This technique is based upon Thellier's laws, which state that pTRMs must be additive (total TRM = sum of pTRMS), independent (pTRM acquired between T1 and T2 is distinct from pTRM acquired between T2 and T3) and reciprocal (the unblocking temperature is the same as the blocking temperature; Thellier 1938; Thellier & Thellier 1959). Results from these types of experiments are often plotted on Arai plots, which depict NRM lost versus pTRM gained (Fig. 2). In an ideal experiment with ideal magnetic recorders, the relationship between NRM lost and pTRM gained is linear, and the slope of the best-fit line to the data is proportional to the intensity of the ancient field. Using this slope, and multiplying by the known lab field, one can calculate the ancient magnetic field

Many results from the Gardar lavas and the Midcontinent Rift do not show this ideal single-slope behaviour, but instead yield curved or double-slope Arai plots, reflecting some form of non-ideal behaviour (Fig. 2). Double-slope Arai plots are difficult to interpret as they can yield two palaeointensity estimates: a higher palaeointensity estimate from the low-temperature portion and a lower palaeointensity estimate from the high-temperature portion.

Proposed causes for double-slope Arai plots include secondary overprints, physiochemical alteration during the laboratory heating and effects related to magnetic recorders that do not obey Thellier's laws such as large pseudo-single-domain (PSD) and multidomain (MD) grain sizes (Valet 2003). Each of these hypotheses can be investigated during palaeointensity experimentation. Secondary overprints are typically associated with directional change that can be identified during demagnetization. In these cases, palaeointensity should only be estimated from temperature steps over which the primary remanence unblocks. However, if the primary remanence is a small fraction of the NRM, it can be difficult to evaluate whether there are deleterious effects from MD remanence carriers influencing the data. Physiochemical alteration can be identified by performing pTRM checks (repeated in-field temperature steps; Thellier & Thellier 1959) throughout the experiment. If a pTRM check differs from the first pTRM step at that temperature, it suggests the sample may be undergoing irreversible alteration to the magnetic mineralogy during heating. In the case of pTRM check failure, it is more appropriate to use part of the Arai diagram not

affected by alteration (i.e. the lower temperature portion). However, one must be careful that the lower temperature portion of the Arai plot is not complicated by effects from MD or large PSD grains, whose effect on the experiment can be difficult to determine when the experiment fails prior to reaching high-temperature steps.

MD and large PSD grains complicate palaeointensity experiments because they can deviate from Thellier's laws. Arguably, Thellier's laws are only fully upheld by non-interacting singledomain (SD) grains. However, the boundary between grain sizes that uphold Thellier's laws and those that violate them is not sharp but instead is transitional with increasing grain size (e.g. Levi 1977). Typical behaviour of MD grains violates Thellier's laws as the blocking temperatures (the temperature required to randomize a portion of the magnetic signal such that a pTRM is acquired in an applied field; $T_{\rm b}$) and unblocking temperatures (temperature necessary to reset the pTRM acquired at $T_{\rm b}$; $T_{\rm ub}$) are not equal, which can result in Arai plot curvature that increases with increasing grain size (Shaskanov & Metallova 1972; Levi 1977; Bol'Shakov & Shcherbakova 1979; Markov et al. 1983; Dunlop & Özdemir 2000, 2001; Shcherbakova et al. 2000; Shcherbakov & Shcherbakova 2001; Xu & Dunlop 2004). Utilizing curved Arai plots for palaeointensity determination can yield large discrepancies in results, with the lower temperature portion of the curve typically yielding overestimates and the higher temperature portion of the curve yielding underestimates, with discrepancies increasing with grain size (Shcherbakov & Shcherbakova 2001; Xu & Dunlop 2004). MD effects can be identified by pTRM tail checks (Riisager & Riisager 2001), which are repeated zero-field temperature steps. Another property of MD grains is a dependence of pTRM on the order of in-field and zero-field steps (Aitken et al. 1988; Valet et al. 1998; Biggin & Böhnel 2003; Tauxe & Staudigel 2004; Yu et al. 2004). This behaviour is well documented within experiments that follow the IZZI protocol, which alternates in-field and zero-field (IZ) and zero-field and in-field steps (ZI), resulting in zigzagging of the Arai plot if MD grains dominate the behaviour (Tauxe & Staudigel 2004; Yu et al. 2004).

A complexity that arises with some double-slope Arai plots is that MD effects may only be evident in the low-temperature portion of the diagram, that is, curving or zigzagging, but then the hightemperature portion of the plot is quasi-linear. Xu & Dunlop (2004) showed that palaeointensity estimates on low- to mid-temperature ranges from such Arai plots yielded overestimates of field strength by as much as 100 per cent for MD magnetite grain sizes and 25 per cent for small PSD magnetite grain sizes. However, palaeointensity estimates made on the quasi-linear medium to high-temperature portion (with f values ≥ 0.5) yielded reasonable field estimates (Xu & Dunlop 2004). This evidence has been used to argue that the high-temperature portion of double-slope Arai plots should be used for palaeointensity determination (e.g. Kulakov et al. 2013a). Recent work by Smirnov et al. (2017) on synthetic samples with known grain sizes of magnetite, showed that for small to moderate size PSD grains (0.75 and 1.5 μ m), palaeointensity estimates determined from the high-temperature portion of double-sloped Arai plots yielded results within ~ 10 per cent of actual field strength (always underestimated), whereas results from the low-temperature slope significantly overestimated the field strength by \sim 70–90 per cent. For larger grain sizes (5–250 μ m), the high-temperature slope resulted in underestimates ranging between 20 and 60 per cent of the original value, and the low-temperature slope overestimated the known applied field by 150-280 per cent. This study also showed that the use of low-temperature demagnetization (LTD) before each heating step in a standard Thellier experiment (LTD-Thellier) helps to straighten Arai plots and can yield more accurate

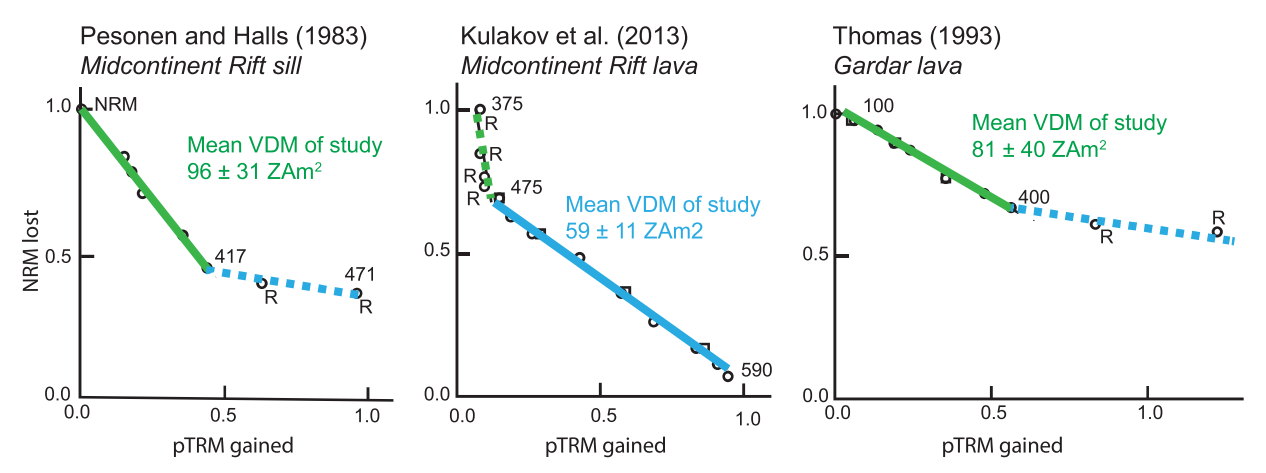


Figure 2. Examples of previously published Arai plots from palaeointensity experiments on the Midcontinent Rift (Pesonen & Halls 1983; Kulakov *et al.* 2013a) and Gardar volcanics (Thomas 1993). While results from all studies have double-slope behaviour, each study interprets the results differently with Pesonen & Halls (1983) and Thomas (1993) using the low-temperature slope as the best representation of the past magnetic field strength and Kulakov *et al.* (2013a) using the high-temperature slope. The green lines mark the low-temperature fits and the blue lines mark the high-temperature fits. The slope used as an estimate in a given study is shown as a solid line while that which was rejected is shown as dashed. Squares mark pTRM checks and *R* indicates points rejected during data analysis. Mean virtual dipole moment values from the studies (not these specific example samples) are annotated on the plots with the mean for the Lake Shore Traps being that reported in Kulakov *et al.* (2013a).

palaeointensity estimates (Smirnov *et al.* 2017). However, for synthetic samples with large PSD and MD grains (12–250 μ m), resulting Arai plots using the LTD-Thellier technique were still double-sloped and estimates of the magnetic field strength from the high-temperature portion underestimated field values by 10–55 per cent (Smirnov *et al.* 2017).

A majority of palaeointensity estimates from Midcontinent Rift and Gardar volcanics were determined from Arai plots with doubleslope behaviour (Pesonen & Halls 1983; Thomas 1993; Kulakov et al. 2013a; Fig. 2). Pesonen & Halls (1983) (Midcontinent Rift, various units) used the low-temperature slopes of their double-slope Arai plots for palaeointensity estimation, suggesting that higher temperature data were affected by physiochemical alteration during heating (Fig. 2). The Thomas (1993) study of Gardar lava flows likewise used the low-temperature slope for palaeointensity determination (Fig. 2). In contrast, the Kulakov et al. (2013a) study of the Lake Shore Traps of the Midcontinent Rift utilized the LTD-Thellier technique and interpreted the higher temperature slope as the best representation of the ancient field strength, suggesting that the low-temperature slopes were biased by large PSD or MD grains. Smirnov et al. (2016) argued that palaeointensity results interpreted from the low-temperature slope of double-slope Arai plots (i.e. Thomas 1993; Pesonen & Halls 1983) are overestimates (per Xu & Dunlop 2004) due to MD effects and viscous remanence. Smirnov (2017) further argued that the results from the Lake Shore Traps data of the Midcontinent Rift (Kulakov et al. 2013a) represent a more accurate estimate of the palaeo-field because that study utilized the LTD-Thellier technique, and calculated palaeointensity from the high-temperature slope of double-slope Arai plots. However, despite the use of the LTD-Thellier method, results from Kulakov et al. (2013a) still show double-slope behaviour (Fig. 2), such that the interpretation of palaeointensity from the high-temperature slope could potentially be an underestimate of the true field strength.

In this study, we seek to develop high-quality palaeointensity estimates for the Osler Volcanic Group and the Mamainse Point volcanics from the Midcontinent Rift to obtain additional constraints on the strength of the geomagnetic field at 1.1 Ga. Given the com-

plexities associated with interpretation of double-slope Arai plots, we seek to develop sufficient data wherein we can solely consider results interpreted from samples showing single-slope behaviour.

2 GEOLOGY

The Osler Volcanic Group and Mamainse Point sequence constitute volcanic products associated with the failed intracontinental Midcontinent Rift System that outcrops throughout the Lake Superior region (Fig. 3; Green 1983; Stein et al. 2015). Volcanism in the Midcontinent Rift was active for \sim 25 Ma, from ca. 1109 (Davis & Sutcliffe 1985) to ca. 1083 Ma (Fairchild et al. 2017), with a total volcanic output greater than 1.5×10^6 km³ that is dominated by basaltic lavas (Hutchinson et al. 1990; Cannon 1992). Magmatism associated with the Midcontinent Rift has been divided into four stages based on changes in relative volcanic volume and nature of magmatism: early (\sim 1109–1105 Ma), latent (\sim 1105–1100 Ma), main (~1100–1094 Ma) and late (<1094 Ma) (Miller & Vervoort 1996; Davis & Green 1997; Vervoort & Green 1997). Volcanic rocks from the Midcontinent Rift have yielded high-quality geochronologic data and palaeomagnetic directional data (e.g. Halls and Pesonen 1982; Davis and Green 1997; Swanson-Hysell et al. 2009, 2014a,b; Tauxe & Kodama 2009; Kulakov et al. 2013b; Fairchild et al. 2017) that have been used to develop a well-resolved apparent polar wander path for Laurentia (cratonic North America) called the Keweenawan Track. The combination of high-quality palaeomagnetic recorders and high-precision geochronology within the Midcontinent Rift provides a robust context for the development and interpretation of palaeointensity data.

2.1 Osler Volcanic Group

Located along the northern part of Lake Superior in Ontario, Canada, the Osler Volcanic Group is a sequence of tholeittic basalt flows that erupted during the early stage of rift magmatism (Swanson-Hysell *et al.* 2014a, Fig. 3). The group overlies

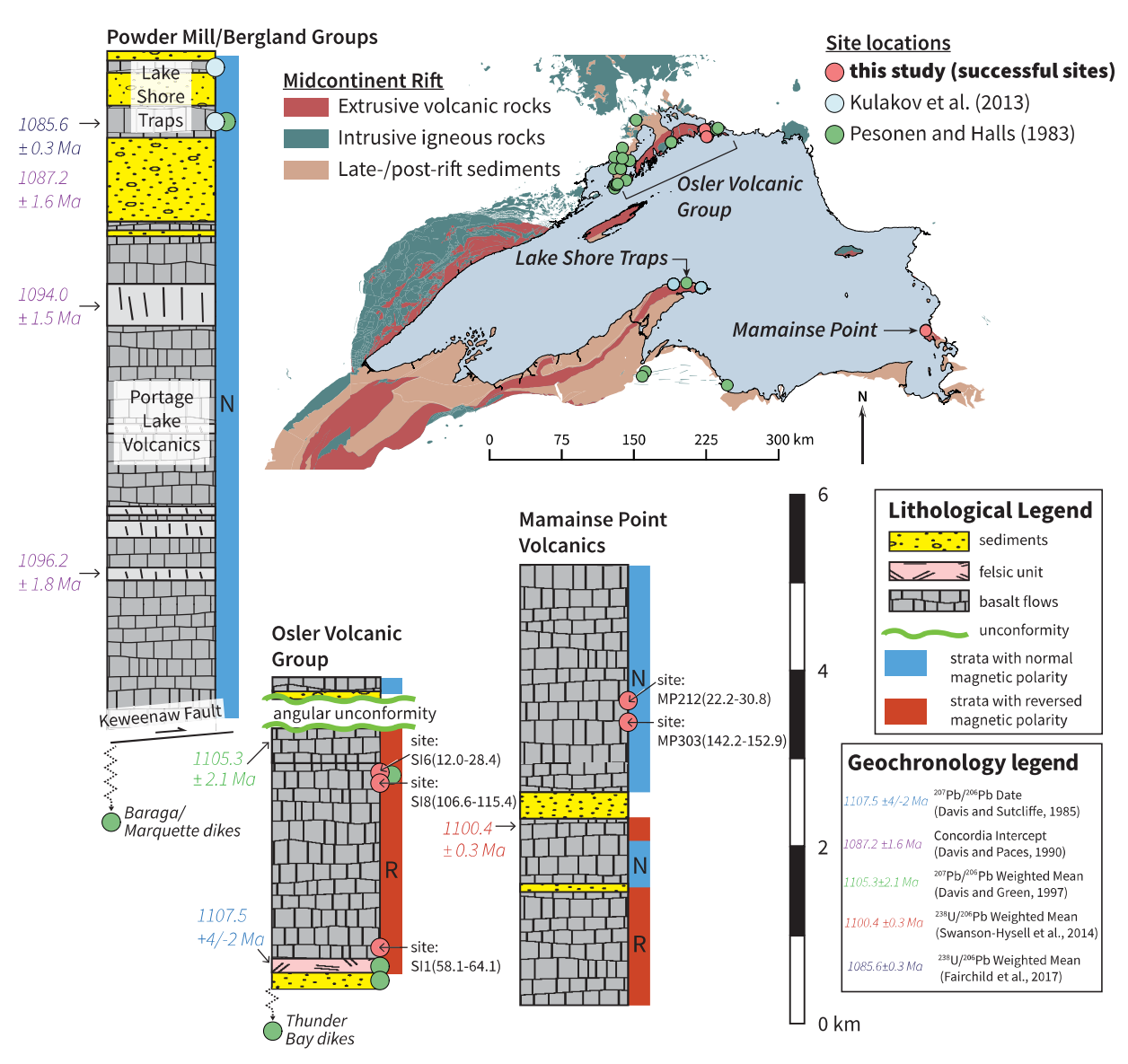


Figure 3. Summary stratigraphic columns for the Lake Shore Traps, Osler Volcanic Group, and Mamainse Point volcanics modified from Fairchild *et al.* (2017). Dates are colour-coded by reference noted in the geochronology legend. Inset shows the distribution of rift and post-rift-related rocks including extrusive, intrusive, and late/post-rift sediments around Lake Superior. Red circles mark sites from this study, blue circles mark sites from Kulakov *et al.* (2013a), and green circles mark sites from Pesonen & Halls (1983).

the epicontinental sediments of the Mesoproterozoic Sibley group (Hollings et al. 2007). Much of the Osler Volcanic Group stratigraphy records reverse polarity, consistent with other rift rocks associated with the early phase of rift magmatism. At Puff Island, an angular unconformity marked by a conglomerate separates lava flows with reverse polarity below from lava flows with normal polarity above (Halls 1974). This conglomerate is associated with a local cessation in magmatic activity which likely corresponds with the latent stage of rift magmatism. Only ~110 m of normally magnetized flows are exposed on Puff Island. Northeast of Puff Island and stratigraphically below the flows exposed there, ~3 km of reversely magnetized flows are exposed on Simpson Island. A U-Pb zircon date reported for an intrusive felsic porphyry intruding the basal Osler Volcanic group provides a minimum age for eruption of 1107.5 \pm 2 Ma (Davis & Sutcliffe 1985). A U-Pb zircon date of 1105 ± 2 Ma for the Agate Point Rhyolite (which is exposed near the top of the reversed polarity flows, stratigraphically higher than flows exposed at Simpson Island) provides a date for the approximate end of early stage volcanism in this region (Davis & Green 1997).

Swanson-Hysell *et al.* (2014a) collected samples from the east shore of Simpson Island where \sim 3000 m of the Osler Volcanic Group are exposed. Palaeomagnetic data from the sequence were interpreted to record a significant decrease in inclination as a result of rapid plate motion (Swanson-Hysell *et al.* 2014a). Based on demagnetization behaviour, 14 flows and 1 dyke were selected from the Osler Volcanic Group for palaeointensity analysis (samples starting with SI; Fig. 3).

2.2 Mamainse Point

The Mamainse Point sequence is a ~4.5-km-thick sequence of volcanic rocks exposed on the northeastern shore of Lake Superior (Ontario, Canada) that unconformably overlies the Archean Superior Province (Fig. 3; Swanson-Hysell *et al.* 2009). Lava flows

Table 1. Quality criteria.

MAD (o)	Beta (per cent)	DANG (o)	FRAC	SCAT	GAP-MAX	N pTRM	N Arai
20	15	5	0.6	TRUE	0.6	2	4

Notes: Criteria used for accepting or rejecting palaeointensity data. See the text for more detail.

range in composition from picrite to basaltic andesite (Shirey 1997). The Mamainse Point sequence is the only location within the rift where multiple reversals (reversed to normal to reversed to normal) are well documented within a section of extrusive basalts (Fig. 3). Palaeomagnetic data developed at Mamainse Point show a progressive decrease in inclination going-up section indicating progressive movement of Laurentia towards the equator (Swanson-Hysell *et al.* 2014b). A U–Pb zircon date of 1100.36 ± 0.25 Ma (2σ analytical uncertainty) collected from a tuff located within the upper reversed portion of the stratigraphy (Swanson-Hysell *et al.* 2014b) provides age constraints on the succession (Fig. 3). For this study, six flows were selected (samples starting with MP) from the upper normal polarity portion of the stratigraphy from those sampled by Swanson-Hysell *et al.* (2009, 2014b, Fig. 3).

3 METHODS

3.1 Sample collection

Sample cores were collected using a hand-held drill and were oriented using a magnetic compass as well as a sun compass when possible. Palaeohorizontal was determined from intercalated sedimentary layers and flow tops. 6-10 cores were drilled from each lava flow in order to robustly determine an accurate site mean. More detailed information about the sites and their context along with directional results are reported in Swanson-Hysell et al. (2009, 2014a,b). For palaeointensity analysis, 5–8 samples per flow were chosen. Samples were chosen based on demagnetization behaviour with a preference for samples wherein relatively little remanence is held by haematite such that their magnetization is dominated by (titano)magnetite recording a primary thermal remanent magnetization. Haematite can be a significant carrier of remanence in Mamainse Point basalts (see Swanson-Hysell et al. 2011) and other successions around the Midcontinent Rift. Given that haematite can form at the expense of magmatic (titano)magnetite, such flows were deemed to not be appropriate targets for the palaeointensity experiments.

3.2 Palaeointensity experimental protocol

A total of 133 specimens from 21 selected sites underwent palaeointensity experiments that followed the stepwise double-heating Thellier method (Thellier & Thellier 1959), using the IZZI protocol (Tauxe & Staudigel 2004). pTRM checks were performed systematically throughout the experiment to test whether there was significant mineralogical alteration due to heating and were assessed using the SCAT parameter of Shaar & Tauxe (2013). All remanence measurements were made on a 2G Enterprises DC-SQUID superconducting rock magnetometer equipped with an automated pick-and-place sample changer system at the UC Berkeley Paleomagnetism laboratory. The magnetometer is housed inside a three-layer magnetostatic shield that maintains background fields of less than 500 nT. Heating steps were performed using an ASC TD-48SC thermal demagnetizer with a controlled field coil that allows for a magnetic field to be generated in the oven in conjunction with a DC power sup-

ply. The thermal demagnetizer was degaussed with an alternating field following 'in-field' steps such that residual fields were < 10 nT during 'zero-field' steps. Samples were placed in the same location within the thermal demagnetizer for each heating step and were maintained in the same orientation with regard to the applied field. During each heating step, samples remained at peak temperatures for 20 min. An applied laboratory field of 30 μ T was used for all infield steps. All heating steps were performed in air. The temperature increments for the experiments were chosen to cover characteristic remanent magnetizations held by (titano)magnetite, with smaller increment temperature steps performed close to the expected unblocking temperature of stoichiometric magnetite. Hysteresis measurements were conducted at the Institute for Rock Magnetism at the University of Minnesota. Major hysteresis loops were measured at room temperature using a Micromag Princeton Measurements vibrating sample magnetometer with nominal sensitivity of $5 \times 10^{-9} \text{ Am}^2$.

The following criteria were used as quality filters on the palaeointensity results: (1) a maximum angular deviation (MAD; Kirschvink 1980) of $<20^{\circ}$; (2) scatter parameter (β ; Coe et al. 1978) values of <15 per cent; (3) a deviation angle (DANG; Tanaka & Kobayashi 2003; Tauxe & Staudigel 2004) of $< 5^{\circ}$; (4) fraction of remanence (FRAC; Shaar & Tauxe 2013) >0.6; (5) scatter statistic (SCAT; Shaar & Tauxe 2013) = TRUE; (6) a maximum gap (GAP-Max; Shaar & Tauxe 2013) < 0.6; (7) number of pTRM checks > 2; (7) and number of measurements used for palaeointensity determination ≥ 4 ; (Table 1). The MAD measures the scatter about the best-fit line through NRM steps in the selected interval for which the intensity is defined. DANG, or deviation angle, is the angle between the best-fit direction that is free floating and the direction between the centre of mass of the data and the origin of the vector component diagram (Tanaka & Kobayashi 2003; Tauxe & Staudigel 2004). Both MAD and DANG assess the directional variation of the NRM, with MAD measuring the scatter in the NRM directions and DANG assessing whether the component is trending toward the origin of the Zijderveld plot. β is the 'scatter' parameter of Coe et al. (1978) and is the ratio of the standard error of the slope of the best-fit line of the selected NRM and pTRM points on an Arai plot to the absolute value of the slope. FRAC is the fraction of the NRM that is used in the best-fit line (Shaar & Tauxe 2013). The FRAC value was chosen to preferentially select samples with dominantly single-slope Arai plots. GAP-Max is the maximum gap between two points on the Arai plot determined by vector arithmetic. SCAT is a Boolean operator which uses the error on the best-fit slope of the selected data on the Arai plot to determine if the data are overly scattered. The parameter is used to assess pTRM checks in addition to assessing the degree to which IZZI steps are zigzagged. β , FRAC, GAP-Max and SCAT are all statistics to assess the behaviour of Arai plots. See the Standard Paleointensity Definitions (Paterson et al. 2014, https://earthref.org/PmagPy/SPD/home.html, last accessed 2018 March 17) for more details. Data analysis was conducted using Thellier GUI (Shaar & Tauxe 2013) within the PmagPy software package (Tauxe et al. 2016). Samples that passed initial criteria listed above were further evaluated using the $Q_{\rm PI}$ quality criteria of Biggin & Paterson (2014). For more details, see Table 2. Q_{PI} scores ≥ 3 were considered successful. All new data at

Table 2. Qualitative reliability criteria (Q_{PI}) .

Flow	N	Age (Ma)	Method	AGE	STAT	TRM	ALT	MD	ACN	TECH	LITH	Q_{PI}
MP212 (22.2–30.8)	6	1096	T+	1	1	1	1	1	1	0	0	6
MP303 (142.1-152.9)	5	1096	T+	1	1	1	1	1	1	0	0	6
SI1 (58.1-64.1)	1	1107.9	T+	1	0	1	1	1	1	0	0	5
SI6 (12.0-28.4)	8	1105.9	T+	1	1	1	1	1	1	0	0	6
SI8 (106.6-115.4)	3	1105.6	T+	1	0	1	1	1	1	0	0	5

Notes: Qualitative reliability criteria (Q_{Pl}) assessment. N indicates the number of specimens used in the palaeointensity estimate for each sample. Age, is the absolute age of the geological unit in Ma. T + indicates the use of a Thellier-type method with pTRM checks. AGE is an assessment of whether the absolute age and palaeomagnetic behaviour are consistent with a reliable palaeointensity estimate, that is, the palaeointensity is derived from a component of remanence that is consistent with the age of the geological unit. STAT is a measure of within site dispersion, and is passed if a minimum of 5 samples per unit have an estimate of true SD/mean \leq 25 per cent. TRM is passed if there is petrographic evidence that the bulk remanence of the sample is likely a thermoremanent magnetization (TRM). ALT is a measure of alteration and is passed if there is reasonable evidence that the samples did not alter during the palaeointensity experiment (pTRM checks). MD is passed if there is reasonable evidence that the final palaeointensity estimate was not biased by multidomain states (pTRM tail checks, curvature of Arai plot, or zigzag of IZZI protocol data). ACN is a check to see whether checks (and corrections if necessary) were made for anisotropy of remanence, cooling rate effects and non-linear remanence. TECH is passed if the palaeointensity estimate was derived from more than one substantially different technique. LITH assesses whether the palaeointensity result is estimated from more than one lithology with significantly different unblocking characteristics. See Biggin and Paterson (2014) for more detailed descriptions.

the measurement level are available within the MagIC database (https://www.earthref.org/MagIC/doi/10.1093/GJI/GGY074) and Arai plots for every analysed specimen are included in the Supporting Information.

4 RESULTS

4.1 Rock magnetism

Hysteresis data are consistent with demagnetization results, which suggest that low-titanium magnetite is a dominant magnetic mineral within our samples (Table S1, Supporting Information). Ratios of summary hysteresis data parameters $(M_r/M_s \text{ and } B_{cr}/B_c)$ show values typically interpreted to indicate PSD magnetite (Fig. S1, Supporting Information). Squareness (M_r/M_s) and coercivity (B_c) values fall along the magnetite line of Wang & Van der Voo (2004) (Fig. S2, Supporting Information). These hysteresis data are consistent with low-titanium magnetite dominating the magnetic mineralogy of the samples. Scanning electron microscopy in conjunction with energy dispersive X-ray spectroscopy conducted on samples from four sites reveal that the iron oxides are titanomagnetite grains comprised of low-titanium magnetite and ilmenite lamellae (see Fig. S4, Supporting Information). Ilmenite intergrowths are present as trellis-type lamellae, sandwich-type laths and composite-type inclusions (terminology following Haggerty 1991). The high-temperature oxyexsolution that formed ilmenite lamellae both lowered the titanium content and the effective grain size of the magnetite grains.

4.2 Palaeointensity

Results from palaeointensity experiments show three dominant behaviours as seen in the Arai plots (Fig. 4): dominantly single-slope/single-direction (17 out of 133 specimens), double-slope/single-direction (30 out of 133 specimens) and sagging and/or zigzagging (64 out of 133 specimens) (Fig. 4). Note that for this classification, distinguishing between double-slope and sagging behaviour can be difficult and is qualitative. Also within the data are 12 specimens that are double-sloped with two directional components and 10 specimens that yielded uninterpretable data. The 23 specimens from five distinct flows passed the quality criteria described above, yielding acceptable palaeointensity estimates for three flows from the Osler Volcanics (42.8, 45.3 and 45.7 μ T;

Table 3) and two from the upper normal of the Mamainse Point lavas (10.4 and 17.5 μ T; Table 3). The quality criteria were constructed to reject double-slope results (FRAC > 0.6) and of the 23 specimens that passed, 17 showed dominantly single-slope Arai plots. Results from six specimens (specimens from flow MP303(142.2–152.9) and specimen SI8–113.6b) did display double-slope behaviour to some degree. The low-temperature, high-slope portion of flow MP303 (142.2–152.9) data is associated with a directional change seen in the Zijderveld plots, consistent with removal of a minor overprint which is followed by the slope that dominates the Arai plots and is used to estimate palaeointensities.

Of the 110 specimens that failed our palaeointensity criteria, 64 failed due to non-ideal behaviour likely resulting from large PSD or MD size grains, as seen from either zigzagging or sagging of the Arai plots (Fig. 4). The 36 samples failed because of double-slope behaviour (resulting in small FRAC) as no component fulfilling the rest of the criteria could be fit in a sizeable fraction of the NRM demagnetization. Of these double-slope specimen results, six can be explained by the presence of two directional components, and 30 have no straightforward explanation but may be due to the behaviour of PSD or MD grains. In experiments that were successful, the samples exhibited a sharp decay of magnetic remanence at temperatures associated with magnetite unblocking which has been shown by Herrero-Bervera & Valet (2009) and Valet *et al.* (2010) to increase fidelity and success rate of Thellier-style palaeointensity experiments.

To further check the reliability of our palaeointensity estimates, we assessed potential biases related to both cooling rate and anisotropy. Experiments have shown that large differences in cooling rate between acquisition of an NRM versus a laboratory pTRM can result in an overestimation for SD grains (Dodson & McClelland-Brown 1980; Halgedahl et al. 1980) or underestimation for MD grains (McClelland-Brown 1984) of the past geomagnetic field strength. To assess the potential effect of cooling rate on our samples, we calculated the rate of cooling for a 10.2 m thick (our maximum flow thickness) basaltic flow using the conductive cooling model of Delaney (1987), through a range of blocking temperatures (500–590 °C) for magnetite. We found a maximum cooling time from an emplacement temperature of 1100 to 500 °C of roughly 2 yr, with a cooling time of roughly 210 d from 590 to 500 °C, corresponding to a cooling rate of 1.1×10^{-5} °C s⁻¹. In comparison, the cooling rate calculated for laboratory steps was $\sim 0.10 \,^{\circ}\text{C s}^{-1}$, 4 orders of magnitude different. If we assume that ideal carriers

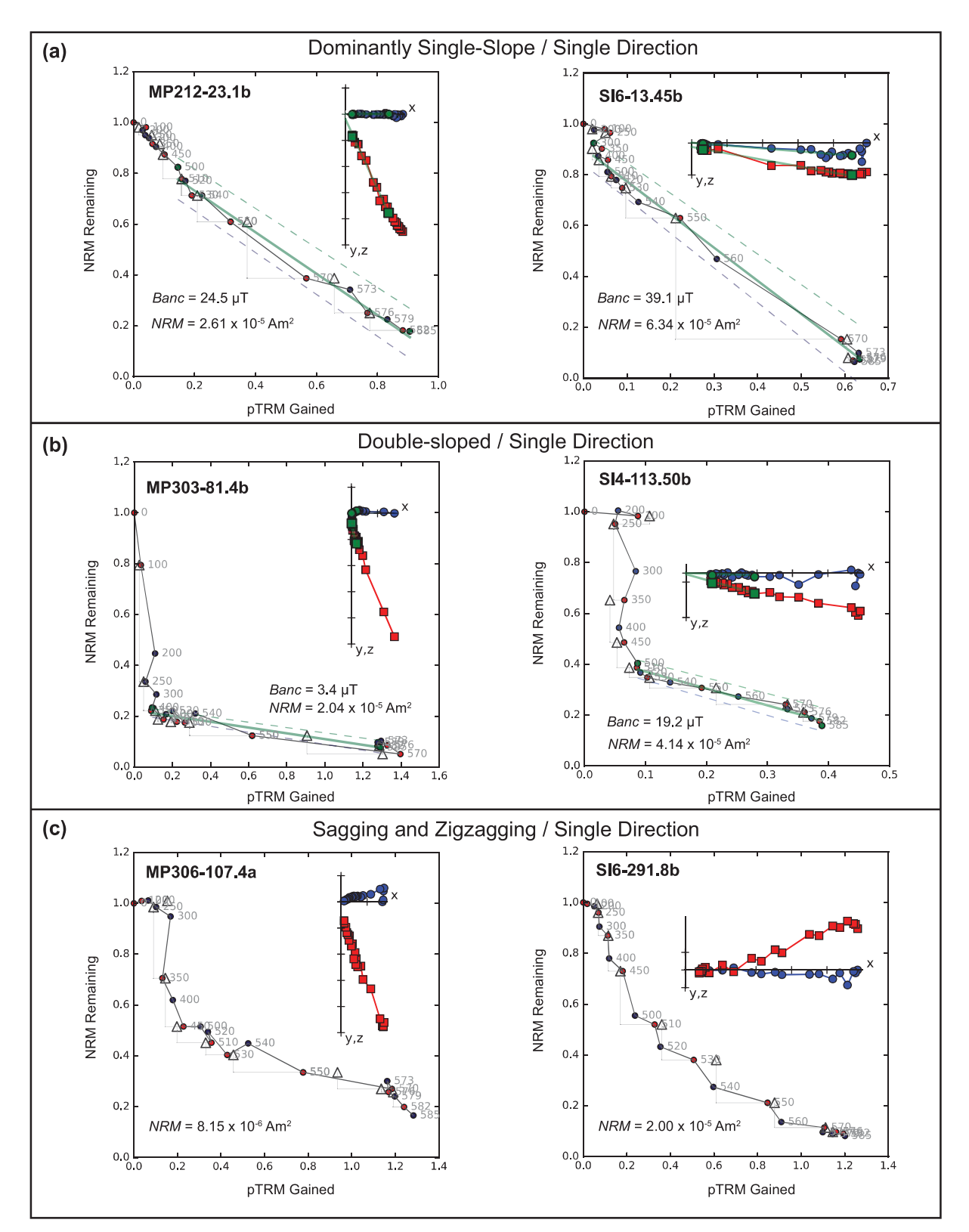


Figure 4. Characteristic results of palaeointensity experiments displayed on Arai and Zijderveld plots (insets) for both Osler Volcanic Group (right) and Mamainse Point Sequence (left) samples. Red (blue) circles indicate zero-field/in-field (in-field/zero-field) steps 'ZI' ('IZ'). Triangles mark pTRM checks. Blue and red squares in the Zijderveld plots are X-Y and X-Z projections, respectively, of the NRMs in specimen coordinates. In these plots, the x-axis is rotated in the direction of the NRM in the X-Y plane. (a) Dominantly single-slope behaviour that passes our acceptance criteria with estimates of the ancient field (B_{anc}) being used to determine site means. (b) Non-ideal double-slope/single-direction behaviour that fails our acceptance criteria. The estimates of the ancient field (B_{anc}) shown are illustrative, but were not deemed acceptable. (c) Non-ideal sagging and zigzagging behaviour that fails our acceptance criteria.

Table 3. Palaeointensity results.

Flow	Specimen	T _{min} (°C)	T _{max} (°C)	Ba	SD Ba	Plat (°)	VDM	SD VDM	Nptrm	DANG (°)	N	FRAC	GAP-MAX	MAD (°)	SCAT	β	γ
MP212 (22.2–30.8)	MP212-22.7b	350	576	15.9					8	1.5	13	0.705	0.223	1.3	Pass	0.041	3.7
MP212 (22.2-30.8)	MP212-22.9b	510	585	19.1					9	0.1	12	0.609	0.273	1.9	Pass	0.035	0.5
MP212 (22.2-30.8)	MP212-23.1b	500	585	24.5					9	1.8	13	0.639	0.247	2.6	Pass	0.032	3.6
MP212 (22.2-30.8)	MP212-24.1b	250	576	14.1					8	2.2	15	0.729	0.205	3.6	Pass	0.040	1.4
MP212 (22.2-30.8)	MP212-24.2b	400	573	16.3					7	2.2	11	0.628	0.247	2.8	Pass	0.050	3.0
MP212 (22.2-30.8)	MP212-25.7b	350	570	15.2					7	1.9	11	0.730	0.304	6.5	Pass	0.045	4.1
Flow mean				17.5	3.8	21.8	38.1	8.3									
MP303 (142.1-152.9)	MP303-149.9b	350	582	10.6					9	3.7	15	0.745	0.182	8.6	Pass	0.034	0.9
MP303 (142.1-152.9)	MP303-148.0b	400	573	9.9					7	2.0	11	0.640	0.233	10.0	Pass	0.044	2.1
MP303 (142.1-152.9)	MP303-147.8b	450	585	9.6					9	3.5	14	0.603	0.235	7.4	Pass	0.043	2.4
MP303 (142.1-152.9)	MP303-148.8b	450	570	9.8					7	1.7	9	0.608	0.293	7.9	Pass	0.058	2.9
MP303 (142.1-152.9)	MP303-149.5b	500	585	12.2					9	2.0	13	0.609	0.204	4.6	Pass	0.039	5.2
Flow mean				10.4	1.1	17.7	23.8	2.5									
SI1 (58.1-64.1)	SI1-61.73b	400	582	45.3					9	3.3	14	0.679	0.152	6.3	Pass	0.052	20.3
Flow mean				45.3	N/A	-46.2	73.2	N/A									
SI6 (12.0-28.4)	SI6-13.35b	400	579	43.3					8	2.5	13	0.601	0.244	4.3	Pass	0.041	15.6
SI6 (12.0-28.4)	SI6-13.45b	300	579	39.1					8	2.1	15	0.737	0.343	2.5	Pass	0.027	2.2
SI6 (12.0-28.4)	SI6-13.50b	500	579	38.5					8	2.2	11	0.611	0.357	4.9	Pass	0.026	3.6
SI6 (12.0-28.4)	SI6-14.20b	400	573	52.8					7	1.6	11	0.650	0.280	4.6	Pass	0.066	21.0
SI6 (12.0-28.4)	SI6-15.00b	500	573	47.2					7	1.8	9	0.603	0.337	4.4	Pass	0.040	13.8
SI6 (12.0-28.4)	SI6-13.36b	450	582	39.5					9	3.3	13	0.607	0.172	5.2	Pass	0.049	19.0
SI6 (12.0-28.4)	SI6-14.40b	400	585	42.6					9	3.1	15	0.613	0.198	4.1	Pass	0.046	12.0
SI6 (12.0-28.4)	SI6-14.45b	400	585	39.1					9	3.3	15	0.608	0.173	3.1	Pass	0.044	9.9
Flow mean				42.8	5.0	-44.5	70.4	8.2									
SI8 (106.6-115.4)	SI8-108.6b	510	579	45					8	0.6	10	0.625	0.376	1.7	Pass	0.063	21.1
SI8 (106.6-115.4)	SI8-109.8b	450	576	47.1					8	0.7	11	0.618	0.407	2.4	Pass	0.048	3.7
SI8 (106.6-115.4)	SI8-113.6b	400	582	44.9					9	0.8	14	0.626	0.173	6.0	Pass	0.085	23.5
Flow mean				45.7	1.2	-47.3	73.0	1.9									

Notes: Palaeointensity results for specimens that passed quality criteria. T_{min} and T_{max} indicate the temperature interval over which the best fit for palaeointensity was defined. Ba indicates the calculated ancient field intensity over the chosen temperature interval in μ T. SD Ba is the standard deviation of the mean flow intensity, measured in μ T. Plat is the palaeolatitude calculated from mean inclination values reported in Swanson-Hysell *et al.* (2009, 2014a,b). VDM is the virtual dipole moment and SD VDM is the standard deviation of the virtual dipole moment reported in ZAm². Nptrm shows the number of pTRM checks within the selected interval for palaeointensity determination. DANG is the deviation angle (DANG). N is the number of steps used within the selected interval for palaeointensity determination. FRAC is the fraction of remanence. GAP-MAX is the maximum gap. MAD is the maximum angle of deviation. SCAT is the scatter parameter (SCAT). β is the scatter parameter. γ is the gamma statistic. Bold text indicates flow mean values.

hold our remanence (i.e. non-interacting SD grains with blocking temperatures close to Curie temperatures) then using the method of Halgedahl *et al.* (1980), we calculate that our estimated field values could overestimate the true field by ~18 per cent. However, our remanence is more likely held by PSD grain sizes than ideal SD carriers, and recent experimental and theoretical models suggest that the cooling rate effect for these grain sizes is negligible (Winklhofer *et al.* 1997; Yu 2011; Biggin *et al.* 2013; Ferk *et al.* 2014). We therefore do not correct our samples for cooling rate, but note that it is a potential source of additional uncertainty.

In order to assess whether our samples are affected by anisotropy of remanence, we calculated the gamma statistic, which is the angular difference between the last pTRM step used for palaeointensity determination and the applied field direction. Our results show gamma values ranging from $\sim 0.5-23.5^{\circ}$, with a median value of 3.7° (Table 3). Considering that these gamma values are typically low, in addition to the fact that anisotropy of remanence is more likely to affect slowly cooled bodies, like plutons, than basaltic lava flows, we do not correct for anisotropy (Selkin et al. 2007). We did not check for non-linear remanence acquisition because this behaviour is most often associated with magnetic particles that exhibit strong shape anisotropy and have needle-like or plate-like habits. Magnetic particles with these habits are commonly found in intrusive bodies as silicate-hosted inclusions, and not in quickly cooled extrusive lava flows (Selkin et al. 2007). As such, our samples are most likely not affected by this phenomenon and we did not correct for it.

All units have Q_{PI} scores (Biggin & Paterson 2014) ranging between 5 and 6 (Table 2). All sites passed AGE, TRM and ALT

(pTRM checks passed and high-temperature steps that looked to be suffering from alteration were excluded), ACN and MD (no significant sagging or zigzagging). Three flows, MP212 (22.2–30.8), MP303 (142.1–152.9) and SI6 (12.0–28.4), met the STAT criterion having \geq 5 specimens with standard deviation/mean values < 0.25. The other flows failed STAT not because the standard deviation/mean was > 0.25, but due to low *N*. None of the sites meet the LITH (multiple lithologies) or TECH (multiple palaeointensity protocols) $Q_{\rm PI}$ criteria.

5 DISCUSSION

5.1 Midcontinent Rift palaeointensity

Palaeointensity estimates for the Osler Volcanic Group (42.8, 45.3 and 45.7 μ T) are stronger than those from the Mamainse Point sequence (10.4 and 17.5 μ T). To assess how much variation in the Midcontinent Rift palaeointensity data may be due to the rapid equatorward motion (\sim 17 cm yr⁻¹) of Laurentia during this time period (Fig. 5b; Fairchild *et al.* 2017), we assumed a constant dipole moment of 74 ZAm² (calculated from Osler Volcanic group palaeointensity estimates) and using this dipole moment calculated the expected change in palaeointensity solely from the latitudinal movement of Laurentia between 1150 and 1080 Ma (Fig. 5a). Comparing the expected change in palaeointensity to all Midcontinent Rift palaeointensity data, including the Abitibi dykes, we see that some of the variation between Midcontinent Rift palaeointensity estimates may be explained by the rapid

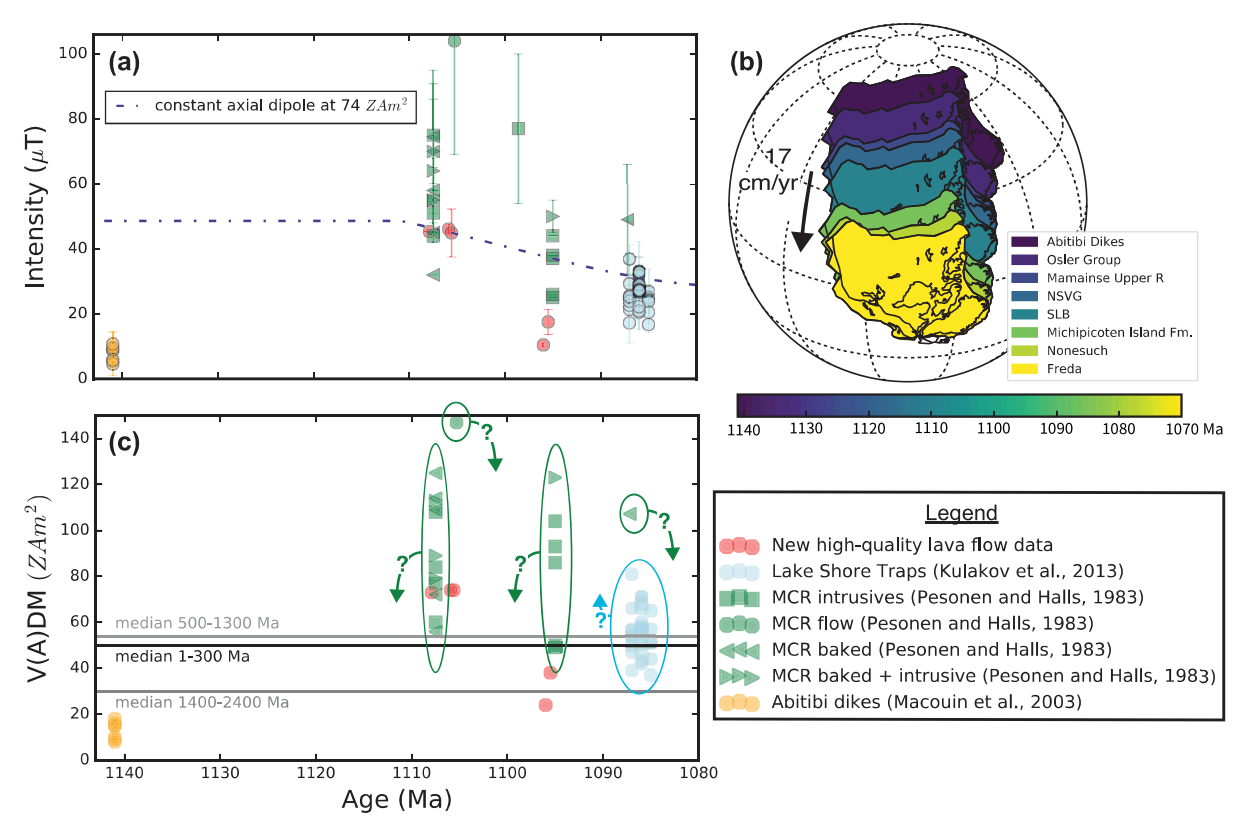


Figure 5. (a) Palaeointensity (in μ T) plotted against age (Ma) for Midcontinent Rift rocks and the Abitibi dykes. The dotted line shows the expected change in palaeointensity due to latitudinal movement of Laurentia between 1150 and 1080 Ma if the axial dipole field was at a constant value of 74 ZAm². (b) Palaeogeographic reconstruction of Laurentia between 1150 and 1080 Ma (modified from Fairchild *et al.* 2017). (c) Magnetic field strength normalized to virtual (axial) dipole moments versus age for Midcontinent Rift rocks and the Abitibi dykes. Grey and black lines show median values for the Mid (2400–1400 Ma), Late (1300–500 Ma) and Recent (300–1 Ma) bins from Biggin *et al.* (2015). Arrows point in direction of what might be the true field if palaeointensity estimates calculated from double-slope Arai plots are overestimates (for data interpreted from low-temperature slopes) or underestimates (for data interpreted from high-temperature slopes). This compilation shows all estimates from Pesonen & Halls (1983) in contrast to Fig. 1 where only the two sites from that study with $Q_{\rm Pl} \geq 3$ are shown.

palaeogeographic change of Laurentia during the late Mesoproterozoic. The remaining difference between palaeointensity values (Fig. 5c) could represent long-term trends in the strength of the magnetic field over this time period, or be the result of secular variation since each flow is a snapshot of the time-varying geomagnetic field.

Using palaeolatitudes calculated from site mean inclination values reported in Swanson-Hysell et al. (2009, 2014a,b), we calculate virtual dipole moments (VDM) from the new palaeointensity estimates shown in Fig. 5 along with previously developed data from the Midcontinent Rift. The calculated mean VDM from the Osler Volcanic Group is $71 \pm 6.8 \text{ ZAm}^2$ and from Mamainse Point is $32 \pm 10 \, \text{ZAm}^2$, with a combined result of $56 \pm 21 \, \text{ZAm}^2$ (all errors are reported at 1 standard deviation). Conducting a Welch's unequal variance *t*-test to test the null hypothesis that two population means are equal reveals the mean of the new data is distinct from Pesonen & Halls (1983) palaeointensity estimates from various units from the Midcontinent Rift, which yield a mean VDM of 96 \pm 31 ZAm². Our new results are consistent with the interpretation that the palaeointensity values from Pesonen & Halls (1983) are overestimated due to being determined from the low-temperature portion of their experiments (Fig. 2). In contrast, the means are indistinguishable between the new data and Kulakov et al.'s (2013a) estimates from the ca. 1085 Ma Lake Shore Traps which have a mean VDM of $56 \pm 10 \, \text{ZAm}^2$. Taken together, our new data and data from Kulakov et al. (2013a) yield a median field strength estimate of 56.0 ZAm²

and a mean of 55.6 ± 12.1 ZAm² for the time period represented by the Midcontinent Rift. While analysis of recent (past 10 Ma) field behaviour shows that large-amplitude variations in field strength on the order of 10 s of ZAm² are possible on such timescales, the overall consistency in the results from this study and that from Kulakov *et al.* (2013a) suggest that ~ 56 ZAm² is a good representation of the average field strength of the Mesoproterozoic geomagnetic field at ca. 1.1 Ga.

Kulakov et al. (2013a) argued that values of this magnitude are consistent with a stable compositionally driven geodynamo operating at 1.1 Ga. The combined Midcontinent Rift estimate is similar to recent estimates of the long-term average field strength during more recent geological time including an estimate of 42 ZAm² from Tauxe et al. (2013, calculated from median values for 5 Ma bins with at least 10 data points meeting selected reliability criteria for the past 140 Ma), and the median value of Biggin et al.'s (2015) 'Recent' (300-1 Ma) bin of 50 ZAm² (Fig. 6a). The mean value of 59.7 \pm 34.3 ZAm² of values in the 300–1 Ma compilation of Biggin et al. (2015) is also consistent with the Midcontinent Rift mean such that the null hypothesis of a common mean between the 1110–1085 Ma values and the 300–1 Ma values cannot be rejected when conducting Welch's unequal variance t-test. This similarity indicates that the surface expression of Earth's geomagnetic field at ca. 1.1 Ga may have been similar in the late Mesoproterozoic to the Mesozoic-Cenozoic, a time period over which we know the inner core existed.

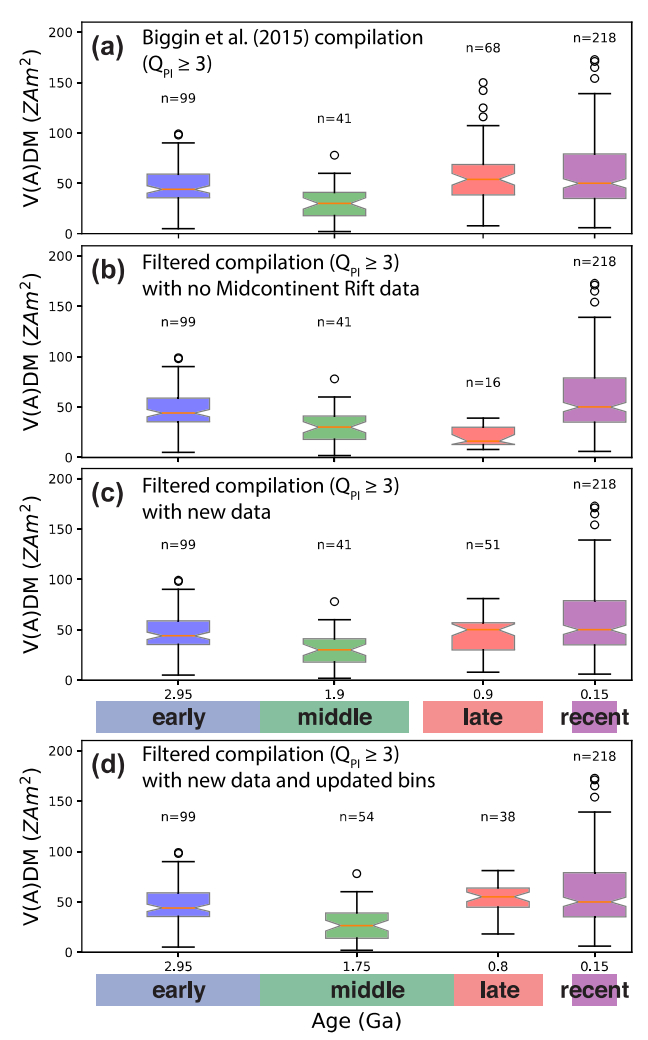


Figure 6. (a) Box plots for early, middle, late and recent time bins (as defined in Biggin *et al.* 2015) for data from the Biggin *et al.* (2015) compilation filtered using $Q_{\rm Pl} \geq 3$ as in the original study. (b) Box plots for the same bins for data with $Q_{\rm Pl} \geq 3$, excluding likely overestimates (Gardar lavas and the Jänisjärvi impact structure) as well as all data from the Midcontinent Rift. This plot illustrates that the interpretation of a Mesoproterozoic increase in field strength is dependent on data from the Midcontinent Rift. (c) Box plots for the compilation excluding potential overestimates and including estimates from this study for the Midcontinent Rift. (d) Same as (c), but using updated time bins. In all plots, horizontal lines and notches are median values, boxes mark the interquartile range (IQR) and error bars show full range excluding outliers (circles) which are defined as being more than 1.51 IQR outside the box. 'n' indicates the number of V(A)DM estimates used in each time interval.

5.2 Precambrian Database Analysis

Whether there are long-term trends in the intensity of the geomagnetic field throughout Earth history is of great interest in understanding the evolution of both Earth's interior and Earth's surface environment. Biggin *et al.* (2015) took the approach of compiling data, assigning these data $Q_{\rm Pl}$ scores, and in their preferred analysis considered the compilation after it was filtered to only include site level estimates with $Q_{\rm Pl} \geq 3$. The data were divided into 'Early' (3500–2400 Ma), 'Mid' (2400–1400 Ma) and 'Late' (1300–500 Ma) time bins with statistical tests, such as the non-parametric Kolmogorov–Smirnov test to evaluate the similarity of the populations of palaeointensity estimates, being applied to compare the populations within the bins. The authors concluded that the 'Early'

and 'Late' bins have significantly higher intensity than the 'Mid' bin with the higher dipole moments in the 'Late' bin being interpreted to be the result of inner core nucleation and the onset of associated compositional convection (Fig. 6a). As discussed in Biggin et al. (2015) and in Smirnov et al. (2016), this interpreted increase is highly dependent upon results from the ca. 1.1. Ga North American Midcontinent Rift (Pesonen & Halls 1983; Kulakov et al. 2013a), and the ca. 1.3 Ga Gardar lava flows from Greenland (Thomas 1993, Figs 1a and 6b). Sites from these two volcanic provinces represent \sim 25 per cent of the total sites with $Q_{\rm PI} \geq 3$ in the Biggin *et al*. (2015) compilation and \sim 75 per cent of those in the 'Late' bin. Unfortunately, much of the data from these localities are from Thellier experiments with non-ideal results manifest in double-sloped Arai plots. While the interpreted late Mesoproterozoic increase in field strength is robust for the removal of data from one locality or the other (Biggin et al. 2015), removing all data from both the Gardar lavas and the Midcontinent Rift would completely eliminate the signal (Fig. 6b). Smirnov et al. (2016) argued that non-ideal results within all of the compiled Gardar lava data and two of the Midcontinent Rift sites that were in the $Q_{PI} \ge 3$ compilation (those of Pesonen & Halls 1983) overestimate the field strength due to their use of the low-temperature slope (Fig. 2), and that as a result the conclusion of an increase in field strength leading into the 1.3–1.1 Ga interval is therefore invalid. While removing these palaeointensity estimates from the compilation is warranted, doing so does not change the conclusions resulting from the statistical analysis if the analysis is conducted at the site (cooling unit) level as is done in Biggin et al. (2015). In fact, the cumulative distributions of palaeointensity estimates in the 'Early' and 'Late' time bins become more similar with removal of these potential overestimates such that using the Kolmogorov-Smirnov test one cannot reject the hypothesis that the distributions of the samples in those bins are the same, and are both distinct from the 'Mid' time bin (see Supporting Information figures presented within the Jupyter notebook found in the Github repository for more details). Even with these overestimates removed, both the 'Early' and 'Late' bins have higher median values, 44 and 48.5 ZAm², respectively, relative to the 'Mid' bin (median of 30 ZAm²). The approach of comparing data at the study or locality level versus at the site level, however, can lead to different conclusions (e.g. Smirnov et al. 2016).

In adding our new data to a quality-filtered compilation for the Precambrian, we take the approach of Biggin et al. (2015) in filtering for sites with $Q_{\rm PI}$ values 3 or greater while also excluding results that have been identified to likely be overestimates due to their determination coming from the low-temperature slopes of double-slope Arai plots (as discussed in Smirnov *et al.* 2016 and Smirnov 2017). This filtering of the sites from the compilation removes the Gardar lava and Midcontinent Rift data of Pesonen & Halls (1983), as discussed above, as well as the palaeointensity estimate from the ca. 682 Ma Jänisjärvi impact structure (Salminen et al. 2006). Evaluating this updated compilation using the time bins as defined in Biggin et al. (2015) results in a updated dipole moment in the 'Late' bin (1300-500 Ma) of 50 ZAm² compared to 44 ZAm² in the 'Early' (3500-2400 Ma) bin and 30 ZAm² in the 'Mid' (2400-1400 Ma) bin (Figs 1b and 6c). The similarity of the populations of VDM between the different time bins can be evaluated using the two sample Kolmogorov-Smirnov test. Results from the Kolmogorov-Smirnov tests show that the distributions of VDMs in the 'Mid' (2400-1400 Ma) and 'Late' (1300-500 Ma) bins are distinct at the 99.9 per cent confidence limit (P = 0.0002), while the null hypothesis that the distribution of VDMs in the 'Late' and 'Early' (3500– 2400 Ma) periods have the same underlying distribution cannot be

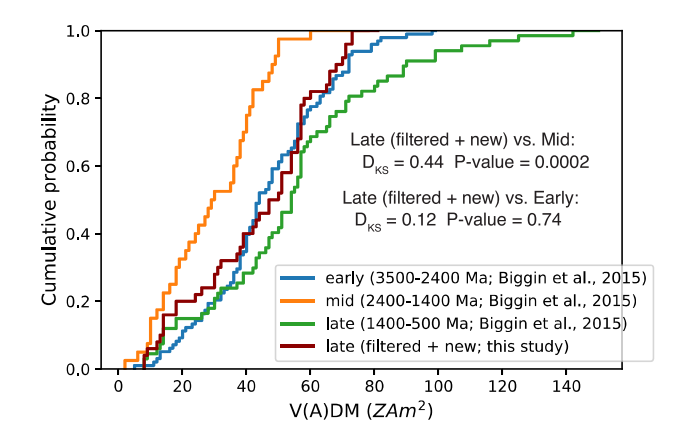


Figure 7. Cumulative distributions of binned palaeointensity estimates using the time bins defined in Biggin *et al.* (2015). The removal of likely overestimates from the 'Late' bin along with the addition of new data results in the distribution increasing in similarity with the 'Early' bin, but remaining quite distinct from the 'Mid' bin as seen in the Kolmogorov–Smirnov test results.

rejected (P = 0.74, Fig. 7). This analysis using the more rigorously filtered compilation along with the new results is consistent with a Mesoproterozoic increase in field intensity when data are analysed at the site level. However, such an increase is entirely dependent upon palaeointensity estimates from the Midcontinent Rift. If data from the Midcontinent Rift were excluded from this updated compilation, an increase in field strength would not be found for the Mesoproterozoic (Fig. 6b).

With the removal of data from the ca. 1.3 Ga Gardar lavas, there are no data in the compilation that would indicate an increase in field strength prior to ca. 1.1 Ga, suggesting that time bins different than those proposed in Biggin et al. (2015) might be more appropriate. Ideally, statistical change-point analysis would be used to develop such bins (e.g. Ingham et al. 2014). However, there are so few estimates for the late Mesoproterozoic and Neoproterozoic (aside from those developed for the Midcontinent Rift) that such an approach cannot currently be robustly conducted. Given that the dipole moments determined from the Midcontinent Rift are higher than those in the preceding 1 Ga, our approach is to keep the 'Early' bin and change the boundary between the 'Mid' and 'Late' bins to be 1100 Ma (Fig. 6d). For these divisions, the 'Early' median is 44.0 ZAm² (3500–2400 Ma, n = 99), the 'Mid' median is 26.5 ZAm^{2} (2400–1100 Ma, n = 54) and the 'Late' median is 55.0 ZAm^{2} (1100–500 Ma, n = 38). Additional palaeointensity data from the Palaeoproterozoic and Mesoproterozoic are needed to further assess the robustness of the low dipole moment values during the 1 Ga preceding the Midcontinent Rift lavas. New data are also needed from the Neoproterozoic to determine whether the relatively high dipole moments from the Midcontinent Rift persisted as might be expected if they are the result of a new and sustained power source to the geodynamo associated with the nucleation of the inner core.

6 CONCLUSIONS

The paucity of Precambrian palaeointensity estimates, as well as non-ideal results within the existing database, present challenges when seeking to interpret long-term trends in the strength of the geomagnetic field. The Midcontinent Rift of North America presents an opportunity to develop robust palaeointensity estimates spanning a $\sim\!25$ Myr interval of the late Mesoproterozoic. Palaeointensity data obtained from the Osler Volcanic Group and the Mamainse Point

sequences of the Midcontinent Rift yield new estimates of the field strength of the ca. 1.1 Ga geomagnetic field. While the majority of the data display non-ideal sagging or double-sloped behaviour, the application of quality filters allows new palaeointensity estimates to be determined from samples that have dominantly single-slope Arai plot behaviour. These data may represent some of the best estimates of the magnetic field strength for this critical time period. Combining these new estimates with data published from the Lake Shore Traps (Kulakov et al. 2013a) yields a median field strength estimate for the time period of Midcontinent Rift development of 56.0 ZAm²—similar to the median dipole moment of palaeointensity estimates for the most recent 300 Myr of Earth history. These data are inconsistent with a weak-field regime operating at the time. That these values are higher than compiled estimates over the preceding billion years, if likely overestimates at 1.3 Ga are removed from the compilation, is suggestive of an increase in surface field intensity prior to 1.1 Ga. However, the interpretation of such an increase is entirely dependent on data from the Midcontinent Rift, and evaluating the robustness of the increase, and whether it was sustained, will require the development of more high-quality palaeointensity data for the Mesoproterozoic and Neoproterozoic Eras. Regardless, the results from the Midcontinent Rift suggest that the strength of the magnetic field at ca. 1.1 Ga was similar to that in geological recent time. Either inner core solidification was a power source to the geodynamo by 1.1 Ga or the dynamics of thermal convection and other potential power sources were able to generate a strong surface field at that time.

ACKNOWLEDGEMENTS

Ontario Parks is acknowledged and thanked for permits to conduct field work within the Lake Superior Archipelago Conservation Reserve. Palaeointensity data for this study are available at the measurement level in the MagIC database (https://www.earthref.org/MagIC/doi/10.1093/GJI/GGY074, last accessed 2018 March 17). Code used for the statistical tests reported in the manuscript is available on Github (https://github.com/Swanson-Hysell-Group/Midcontinent_Rift_Paleointensity/, last accessed 2018 March 17).

FUNDING

This research was supported by the National Science Foundation under grants EAR-1045635 and EAR-1419894 awarded to NLS-H.

REFERENCES

Aitken, M.J., Allsop, A.L., Bussell, G.D. & Winter, M.B., 1988. Determination of the intensity of the Earth's magnetic field during archaeological times: reliability of the Thellier Technique, *Rev. Geophys.*, **26**(1), 3–12.

Aubert, J., Labrosse, S. & Poitou, C., 2009. Modelling the palaeo-evolution of the geodynamo, *Geophys. J. Int.*, **179**(3), 1414–1428.

Badro, J., Siebert, J. & Nimmo, F., 2016. An early geodynamo driven by exsolution of mantle components from Earth's core, *Nature*, **536**(7616), 326–328.

Biggin, A.J. & Böhnel, H.N., 2003. A method to reduce the curvature of Arai plots produced during Thellier palaeointensity experiments performed on multidomain grains, *Geophys. J. Int.*, 155(3), F13–F19.

Biggin, A.J. & Paterson, G.A., 2014. A new set of qualitative reliability criteria to aid inferences on palaeomagnetic dipole moment variations through geological time, *Geomagn. Paleomagn.*, **2**(24), doi:10.3389/feart.2014.00024.

- Biggin, A.J., Strik, G. & Langereis, C.G., 2009. The intensity of the geomagnetic field in the late-Archaean: new measurements and an analysis of the updated IAGA palaeointensity database, *Earth Planets Space EPS*, **61**(1), 9–22.
- Biggin, A.J., Badejo, S., Hodgson, E., Muxworthy, A.R., Shaw, J. & Dekkers, M.J., 2013. The effect of cooling rate on the intensity of thermoremanent magnetization (TRM) acquired by assemblages of pseudo-single domain, multidomain and interacting single-domain grains, *Geophys. J. Int.*, 193(3), 1239–1249.
- Biggin, A.J., Piispa, E.J., Pesonen, L.J., Holme, R., Paterson, G.A., Veikkolainen, T. & Tauxe, L., 2015. Palaeomagnetic field intensity variations suggest Mesoproterozoic inner-core nucleation, *Nature*, 526(7572), 245–248.
- Bol'Shakov, A.S. & Shcherbakova, V.V., 1979. A thermomagnetic criterion for determining the domain structure of ferrimagnetics, *Izv. Acad. Sci. USSR Phys.*, **15**, 111–117.
- Cannon, W.F., 1992. The Midcontinent rift in the Lake Superior region with emphasis on its geodynamic evolution, *Tectonophysics*, **213**(1–2), 41–48.
- Coe, R.S., Grommé, S. & Mankinen, E.A., 1978. Geomagnetic paleointensities from radiocarbon-dated lava flows on Hawaii and the question of the Pacific nondipole low, *J. geophys. Res.*, **83**(B4), 1740–1756.
- Davies, C.J., 2015. Cooling history of Earth's core with high thermal conductivity, *Phys. Earth planet. Inter.*, 247, 65–79.
- Davis, D.W. & Green, J.C., 1997. Geochronology of the North American Midcontinent rift in western Lake Superior and implications for its geodynamic evolution, *Can. J. Earth Sci.*, 34(4), 476–488.
- Davis, D.W. & Sutcliffe, R.H., 1985. U-Pb ages from the Nipigon plate and northern Lake Superior, *Bull. geol. Soc. Am.*, **96**(12), 1572–1579.
- de Koker, N., Steinle-Neumann, G. & Vlček, V., 2012. Electrical resistivity and thermal conductivity of liquid Fe alloys at high P and T, and heat flux in Earth's core, *Proc. Natl. Acad. Sci.*, 109(11), 4070–4073.
- Delaney, P.T., 1987. Heat transfer during emplacement and cooling of mafic dykes, *Mafic Dyke Swarms*, **34**, 31–46.
- Dodson, M.H. & McClelland-Brown, E., 1980. Magnetic blocking temperatures of single-domain grains during slow cooling, *J. geophys. Res.*, 85(B5), 2625–2637.
- Driscoll, P.E., 2016. Simulating 2 Ga of geodynamo history, Geophys. Res. Lett., 43(11), 5680–5687.
- Dunlop, D.J. & Özdemir, Ö., 2000. Effect of grain size and domain state on thermal demagnetization tails, Geophys. Res. Lett., 27(9), 1311–1314.
- Dunlop, D.J. & Özdemir, Ö., 2001. Beyond Néel's theories: thermal demagnetization of narrow-band partial thermoremanent magnetizations, *Phys. Earth planet. Inter.*, **126**(1–2), 43–57.
- Fairchild, L.M., Swanson-Hysell, N.L., Ramezani, J., Sprain, C.J. & Bowring, S.A., 2017. The end of Midcontinent Rift magmatism and the paleogeography of Laurentia, *Lithosphere*, L580.1, doi:10.1130/L580.1.
- Ferk, A., Leonhardt, R., Hess, K.-U., Koch, S., Egli, R., Krása, D. & Dingwell, D.B., 2014. Influence of cooling rate on thermoremanence of magnetite grains: identifying the role of different magnetic domain states, *J. geophys. Res.*, 119(3), 1599–1606.
- Gomi, H., Ohta, K., Hirose, K., Labrosse, S., Caracas, R., Verstraete, M.J. & Hernlund, J.W., 2013. The high conductivity of iron and thermal evolution of the Earth's core, *Phys. Earth planet. Inter.*, **224**, 88–103.
- Green, J.C., 1983. Geologic and geochemical evidence for the nature and development of the middle Proterozoic (Keweenawan) Midcontinent Rift of North America, *Tectonophysics*, 94(1–4), 413–437.
- Gubbins, D., Alfè, D., Masters, G., Price, G.D. & Gillan, M., 2004. Gross thermodynamics of two-component core convection, *Geophys. J. Int.*, 157(3), 1407–1414.
- Haggerty, S.E., 1991. Oxide textures; a mini atlas, *Rev. Mineral. Geochem.*, **25**, 129–219.
- Halgedahl, S.L., Day, R. & Fuller, M., 1980. The effect of cooling rate on the intensity of weak-field trm in single-domain magnetite, *J. geophys. Res.*, 85(B7), 3690–3698.
- Halls, H.C., 1974. A paleomagnetic reversal in the osler volcanic group, Northern Lake Superior, Can. J. Earth Sci., 11(9), 1200–1207.
- Halls, H. & Pesonen, L., 1982. Paleomagnetism of Keweenawan rocks, Geol. Soc. Am. Mem., 156, 172–201.

- Herrero-Bervera, E. & Valet, J.P., 2009. Testing determinations of absolute paleointensity from the 1955 and 1960 Hawaiian flows. *Earth planet. Sci. Lett.*, **287**(3–4), 420–433.
- Hirose, K., Morard, G., Sinmyo, R., Umemoto, K., Hernlund, J., Helffrich, G. & Labrosse, S., 2017. Crystallization of silicon dioxide and compositional evolution of the Earth's core, *Nature*, 543(7643), 99–102.
- Hollings, P., Fralick, P. & Cousens, B., 2007. Early history of the Midcontinent Rift inferred from geochemistry and sedimentology of the Mesoproterozoic Osler Group, northwestern Ontario. *Can. J. Earth Sci.*, 44(3), 389–412.
- Hutchinson, D.R., White, R.S., Cannon, W.F. & Schulz, K.J., 1990. Keweenaw hot spot: geophysical evidence for a 1.1 Ga mantle plume beneath the Midcontinent Rift System, *J. geophys. Res.*, 95(B7), 10 869–10 884.
- Ingham, E., Heslop, D., Roberts, A.P., Hawkins, R. & Sambridge, M., 2014.
 Is there a link between geomagnetic reversal frequency and paleointensity? A Bayesian approach, *J. geophys. Res.*, 119, 5290–5304.
- Jacobs, J.A., 1953. The Earth's Inner Core, *Nature*, **172**(4372), 297–298.
- Kirschvink, J.L., 1980. The least-squares line and plane and the analysis of palaeomagnetic data, *Geophys. J. Int.*, **62**(3), 699–718.
- Konôpková, Z., McWilliams, R.S., Gómez-Pérez, N. & Goncharov, A.F., 2016. Direct measurement of thermal conductivity in solid iron at planetary core conditions, *Nature*, **534**(7605), 99–101.
- Kulakov, E.V., Smirnov, A.V. & Diehl, J.F., 2013. Absolute geomagnetic paleointensity as recorded by ~1.09 Ga Lake Shore Traps (Keweenaw Peninsula, Michigan), *Stud. Geophys. Geod.*, **57**(4), 565–584.
- Kulakov, E.V., Smirnov, A.V. & Diehl, J.F., 2013. Paleomagnetism of ~1.09 Ga Lake Shore Traps (Keweenaw Peninsula, Michigan): new results and implications. *Can. J. Earth Sci.*, **50**(11), 1085−1096.
- Labrosse, S., 2015. Thermal evolution of the core with a high thermal conductivity, *Phys. Earth planet. Inter.*, **247**, 36–55.
- Landeau, M., Aubert, J. & Olson, P., 2017. The signature of inner-core nucleation on the geodynamo, *Earth planet. Sci. Lett.*, 465, 193–204.
- Levi, S., 1977. The effect of magnetite particle size on paleointensity determinations of the geomagnetic field, *Phys. Earth planet. Inter.*, 13(4), 245–259.
- Markov, G.P., Shcherbakov, V.P., Bolshakov, A.S. & Vinogradov, Y.K., 1983.
 On the temperature dependence of the partial thermoremanent magnetization of multidomain grains, *Izv. Acad. Sci. Earth Phys.*, 19, 625–630.
- McClelland-Brown, E., 1984. Experiments on TRM Intensity Dependence on Cooling Rate, *Geophys. Res. Lett.*, **11**(3), 205–208.
- Miller, J.D. & Vervoort, J.D., 1996. The latent magmatic stage of the Midcontinent Rift: A period of magmatic underplating and melting of the lower crust, *Institute on Lake Superior Geology Proceedings*, 42, 33–35.
- O'Rourke, J.G. & Stevenson, D.J., 2016. Powering Earth's dynamo with magnesium precipitation from the core, *Nature*, **529**(7586), 387–389.
- O'Rourke, J.G., Korenaga, J. & Stevenson, D.J., 2017. Thermal evolution of Earth with magnesium precipitation in the core, *Earth planet. Sci. Lett.*, **458**, 263–272.
- Ohta, K., Kuwayama, Y., Hirose, K., Shimizu, K. & Ohishi, Y., 2016. Experimental determination of the electrical resistivity of iron at Earth's core conditions. *Nature*, 534(7605), 95–98.
- Olson, P., 2013. The new core paradox, *Science*, 342(6157), 431–432.
- Paterson, G.A., Tauxe, L., Biggin, A.J., Shaar, R. & Jonestrask, L.C., 2014.
 On improving the selection of Thellier-type paleointensity data. *Geochem. Geophys. Geosyst.*, 15(4), 1180–1192.
- Pesonen, L.J. & Halls, H.C., 1983. Geomagnetic field intensity and reversal asymmetry in late Precambrian Keweenawan rocks, *Geophys. J. Int.*, 73(1), 241–270.
- Pozzo, M., Davies, C., Gubbins, D. & Alfè, D., 2012. Thermal and electrical conductivity of iron at Earth's core conditions, *Nature*, **485**(7398), 355–358
- Riisager, P. & Riisager, J., 2001. Detecting multidomain magnetic grains in Thellier palaeointensity experiments, *Phys. Earth planet. Inter.*, **125**(1–4), 111–117.
- Salminen, J., Donadini, F., Pesonen, L.J., Masaitis, V.L. & Naumov, M.V., 2006. Paleomagnetism and petrophysics of the Jänisjärvi impact structure, Russian Karelia, *Meteorit. Planet. Sci.*, 41(12), 1853–1870.

- Selkin, P.A., Gee, J.S. & Tauxe, L., 2007. Nonlinear thermoremanence acquisition and implications for paleointensity data, *Earth planet. Sci. Lett.*, 256(1–2), 81–89.
- Shaar, R. & Tauxe, L., 2013. Thellier GUI: an integrated tool for analyzing paleointensity data from Thellier-type experiments, *Geochem. Geophys. Geosyst.*, 14(3), 677–692.
- Shaskanov, V.A. & Metallova, V.V., 1972. Violation of Thellier's law for partial thermoremanent magnetizations, *Izv. Phys.*, 8, 180–184.
- Shcherbakov, V.P. & Shcherbakova, V.V., 2001. On the suitability of the Thellier method of palaeointensity determinations on pseudo-single-domain and multidomain grains, *Geophys. J. Int.*, **146**(1), 20–30.
- Shcherbakova, V.V., Shcherbakov, V.P. & Heider, F., 2000. Properties of partial thermoremanent magnetization in pseudosingle domain and multidomain magnetite grains, *J. geophys. Res.*, **105**(B1), 767–781.
- Shirey, S.B., 1997. Re-Os isotopic compositions of Midcontinent rift system picrites: implications for plume – lithosphere interaction and enriched mantle sources, *Can. J. Earth Sci.*, 34(4), 489–503.
- Smirnov, A.V., 2017. Intensity of geomagnetic field in the Precambrian and evolution of the Earth's deep interior. *Izv. Phys.*, 53(5), 760–768.
- Smirnov, A.V., Tarduno, J.A., Kulakov, E.V., McEnroe, S.A. & Bono, R.K., 2016. Palaeointensity, core thermal conductivity and the unknown age of the inner core, *Geophys. J. Int.*, 205(2), 1190–1195.
- Smirnov, A.V., Kulakov, E.V., Foucher, M.S. & Bristol, K.E., 2017, Intrinsic paleointensity bias and the long-term history of the geodynamo, *Sci. Adv.*, **3**(2), e1602306, doi: 10.1126/sciadv.1602306.
- Stein, C.A., Kley, J., Stein, S., Hindle, D. & Keller, G.R., 2015. North America's Midcontinent Rift: when rift met LIP, Geosphere, 11(5), 1607– 1616.
- Stevenson, D.J., Spohn, T. & Schubert, G., 1983. Magnetism and thermal evolution of the terrestrial planets, *Icarus*, **54**(3), 466–489.
- Swanson-Hysell, N.L., Maloof, A.C., Weiss, B.P. & Evans, D.A.D., 2009. No asymmetry in geomagnetic reversals recorded by 1.1-billion-year-old Keweenawan basalts, *Nat. Geosci.*, 2(10), 713–717.
- Swanson-Hysell, N.L., Feinberg, J.M., Berquó, T.S. & Maloof, A.C., 2011. Self-reversed magnetization held by martite in basalt flows from the 1.1-billion-year-old Keweenawan rift, Canada, *Earth planet. Sci. Lett.*, 305(1–2), 171–184.
- Swanson-Hysell, N.L., Vaughan, A.A., Mustain, M.R. & Asp, K.E., 2014. Confirmation of progressive plate motion during the Midcontinent Rift's early magmatic stage from the Osler Volcanic Group, Ontario, Canada, Geochem. Geophys. Geosyst., 15(5), 2039–2047.
- Swanson-Hysell, N.L., Burgess, S.D., Maloof, A.C. & Bowring, S.A., 2014.
 Magmatic activity and plate motion during the latent stage of Midcontinent Rift development, *Geology*, 42(6), 475–478.
- Tanaka, H. & Kobayashi, T., 2003. Paleomagnetism of the late Quaternary Ontake Volcano, Japan: directions, intensities, and excursions, *Earth Planets Space*, 55(4), 189–202.
- Tauxe, L. & Kodama, K.P., 2009. Paleosecular variation models for ancient times: clues from Keweenawan lava flows, *Phys. Earth planet. Inter.*, 177(1–2), 31–45.
- Tauxe, L. & Staudigel, H., 2004. Strength of the geomagnetic field in the Cretaceous Normal Superchron: new data from submarine basaltic glass of the Troodos Ophiolite, *Geochem. Geophys. Geosyst.*, 5(2), Q02H06, doi:10.1029/2003GC000635.
- Tauxe, L., Gee, J.S., Steiner, M.B. & Staudigel, H., 2013. Paleointensity results from the Jurassic: new constraints from submarine basaltic glasses of ODP Site 801C, Geochem. Geophys. Geosyst., 14(10), 4718–4733.
- Tauxe, L. et al., 2016. PmagPy: software package for paleomagnetic data analysis and a bridge to the Magnetics Information Consortium (MagIC) Database, Geochem. Geophys. Geosyst., 17(6), 2450–2463.
- Thellier, E., 1938. On the magnetization of bricks and pottery, *Ann. Phys.*, **16**, 157–302.
- Thellier, E. & Thellier, O., 1959. On the Intensity of the Earth's magnetic field in the historical and geological past, *Izv. Akad. Nauk. SSSR Ser. Geofiz.*, **9**, 1296–1331.
- Thomas, N., 1993, An integrated rock magnetic approach to the selection or rejection of ancient basalt samples for palaeointensity experiments *Phys. Earth planet. Inter.*, **75**(4), 329–342.

- Valet, J.-P., 2003. Time variations in geomagnetic intensity, *Rev. Geophys.*, **41**(1), doi:10.1029/2001RG000104.
- Valet, J.-P., Kidane, T., Soler, V., Brassart, J., Courtillot, V. & Meynadier, L., 1998. Remagnetization in lava flows recording pretransitional directions, *J. geophys. Res.*, 103(B5), 9755–9775.
- Valet, J.P., Herrero-Bervera, E., Carlut, J. & Kondopoulou, D., 2010. A selective procedure for absolute paleointensity in lava flows. *Geophys. Res. Lett.*, 37(16), L16308, doi:10.1029/2010GL044100.
- Valet, J.-P., Besse, J., Kumar, A., Vadakke-Chanat, S. & Philippe, E., 2014.
 The intensity of the geomagnetic field from 2.4 Ga old Indian dykes,
 Geochem. Geophys. Geosyst., 15(6), 2426–2437.
- Verhoogen, J., 1961. Heat balance of the Earth's core, *Geophys. J. Int.*, 4(s0), 276–281.
- Vervoort, J.D. & Green, J.C., 1997. Origin of evolved magmas in the Midcontinent rift system, northeast Minnesota: Nd-isotope evidence for melting of Archean crust, *Can. J. Earth Sci.*, 34(4), 521–535.
- Wang, D. & Van der Voo, R., 2004. The hysteresis properties of multidomain magnetite and titanomagnetite/titanomagnemite in mid-ocean ridge basalts, *Earth planet. Sci. Lett.*, 220(1–2), 175–184.
- Winklhofer, M., Fabian, K. & Heider, F., 1997. Magnetic blocking temperatures of magnetite calculated with a three-dimensional micromagnetic model, *J. geophys. Res.*, **102**(B10), 22695–22709.
- Xu, S. & Dunlop, D.J., 2004, Thellier paleointensity theory and experiments for multidomain grains, *J. geophys. Res.*, 109(B7), B07103, doi:10.1029/2004JB003024.
- Yu, Y., 2011. Importance of cooling rate dependence of thermoremanence in paleointensity determination, *J. geophys. Res.*, 116(B9), B09101, doi:10.1029/2011JB008388.
- Yu, Y., Tauxe, L. & Genevey, A., 2004. Toward an optimal geomagnetic field intensity determination technique, *Geochem. Geophys. Geosyst.*, 5(2), Q02H07, doi:10.1029/2003GC000630.

SUPPORTING INFORMATION

Supplementary data are available at *GJI* online.

- **Figure S1.** Day plot of hysteresis data $(M_r/M_s \text{ versus } B_{cr}/B_c)$ for select samples. Flows that passed (failed) palaeointensity criteria are shown in dark blue (light blue).
- **Figure S2.** Squareness (M_r/M_s) versus coercivity $(B_c$, measured in mT) plot of the same samples plotted in Fig. S1. Dark blue and light blue lines show trends for TM60 and low-Ti magnetite after Wang & Van der Voo (2004).
- **Figure S3.** Results of palaeointensity experiments displayed on Arai plots and Zijderveld plots (insets) for all data. Data shown with $B_{\rm anc}$ estimates passed quality criteria. Red (blue) circles indicate zero-field/in-field (in-field/zero-field) steps 'ZI' ('IZ'). Triangles mark pTRM checks. Blue and red squares in the Zijderveld plots are X-Y and X-Z projections, respectively, of the NRMs in specimen coordinates. In these plots, the x-axis is rotated in the direction of the NRM in the X-Y plane.
- **Figure S4.** Scanning electron microscope (SEM) photomicrographs of (titano)magnetite grains from sampled flows that passed the quality control criteria (Table 3). Grains exhibit Ti-poor magnetite bounded by ilmenite exsolution structures in the form of trellistype lamellae, sandwich-type lamellae, or a composite of these two types (Haggerty 1991). Trellis-type lamellae consist of thin, dense, cross-cutting intergrowths of ilmenite (e.g. b, c and e), whereas sandwich-type lamellae are thicker bands of exsolved ilmenite that tend to exhibit a single preferred orientation (e.g. h, i and j). Both of these types may be present in the same titanomagnetite grain (e.g. a, d, f, g, k and l), and both are thought to be associated with deuteric oxidation. Although our palaeointensity measurements are

Downloaded from https://academic.oup.com/gji/article-abstract/213/3/1969/4904178 by University Of Minnesota user on 02 January 2019

likely concerned only with titanomagnetite grains smaller than those pictured here (micrometres to submicrometres size), these features suggest that magnetite in these flows preserves a primary thermal remanent magnetization (TRM).

Table S1. Hysteresis parameters for flows from the Osler Volcanic Group and Mamainse Point Volcanic Group that were used for palaeointensity determination. M_s is saturation magnetization, M_r is saturation remanent magnetization, B_c is coercivity and B_{cr} is

coercivity of remanence. * indicates that the sample was used for palaeointensity determination.

Please note: Oxford University Press are not responsible for the content or functionality of any supporting materials supplied by the authors. Any queries (other than missing material) should be directed to the corresponding author for the paper.